Available online at www.sciencedirect.com
ScienceDirect
Estuarine, Coastal and Shelf Science 72 (2007) 129–137
ESTUARINE COASTAL AND SHELF SCIENCE
www.elsevier.com/locate/ecss

Comparison of observed (HF radar, ADCP) and model barotropic tidal currents in the New York Bight and Block Island Sound

Jenq-Chi Mau [a], Dong-Ping Wang [a,*], David S. Ullman [b], Daniel L. Codiga [b]

[a] *Marine Sciences Research Center, Stony Brook University, Stony Brook, NY 11794, USA*
[b] *Graduate School of oceanography, University of Rhode Island, Narragansett, RI 02882, USA*

Received 21 June 2006; accepted 14 October 2006
Available online 4 December 2006

Abstract

A three-dimensional, primitive-equation model is used to simulate the barotropically-forced semidiurnal tidal currents in the New York Bight (NYB) and Block Island Sound (BIS). Model tidal velocity ellipses are verified at historical current meter locations and with measurements from acoustic Doppler current profilers (ADCPs) and HF radar (CODAR). The model reproduces well the regional tidal flow pattern as well as the vertical tidal velocity structure. The model misfits typically are 2–4 cm/s in amplitude and 5–7° in orientation. Through comprehensive skill assessment, the model's capacity of simulating the three-dimensional barotropic tidal currents is clearly demonstrated. Moreover, it is shown that the integrity of HF radar measurements can be assured by verifying with model tidal ellipses.

Keywords: HF radar; tidal model; New York Bight; Block Island Sound; skill assessment

1. Introduction

The need for model skill assessment has long been recognized. However, apart from the water levels (tide, storm surge), model predictions rarely have been quantitatively evaluated with the observations (Lynch and Davis, 1995). Instead, ''most coastal current modeling studies use observations only to motivate the research or identify some general features reproduced'' (Whitney and Garvine, 2006). The problem, we think, lies in the lack of ''mutual interest'' between models and observations. The field studies, on the one hand, scarcely strive to synthesize massive dataset into a few useful (to the model) numbers. The model studies, on the other hand, often employ less than adequate forcing (and initial condition) data to render the simulation realistic.

Nowadays coastal ocean models are routinely put into operational use. To insure the scientific integrity, it is vital that the model products are skill assessed. In this study, we make a comprehensive evaluation of a three-dimensional model of the barotropic tidal currents in the New York Bight (NYB) and Block Island Sound (BIS). The flow structure is three-dimensional and its dynamics frictional; this differs from two-dimensional models which are based on vertically averaged hydrodynamics. The data used in the study includes an extensive array of moored current meters and ADCPs, and HF radar. We focus on comparison of the horizontal and vertical structures of the tidal ellipses. We also compare the model and radar-derived tidal ellipses to assess the quality of radar measurements.

In Section 2, the study area is described. In Section 3, sea level and velocity data are analyzed. In Section 4, the three-dimensional tidal model is introduced. In Sections 5, model results are verified with the sea levels, current meters, and ADCPs. In Section 6, model results are compared with the HF radars. In Section 7, the results are discussed.

2. Study area

The Block Island Sound (BIS) is situated at the junction of the Long Island Sound (LIS) and the inner shelf of the New

* Corresponding author.
E-mail address: dong-ping.wang@sunysb.edu (D.-P. Wang).

0272-7714/$ - see front matter © 2006 Elsevier Ltd. All rights reserved.
doi:10.1016/j.ecss.2006.10.011

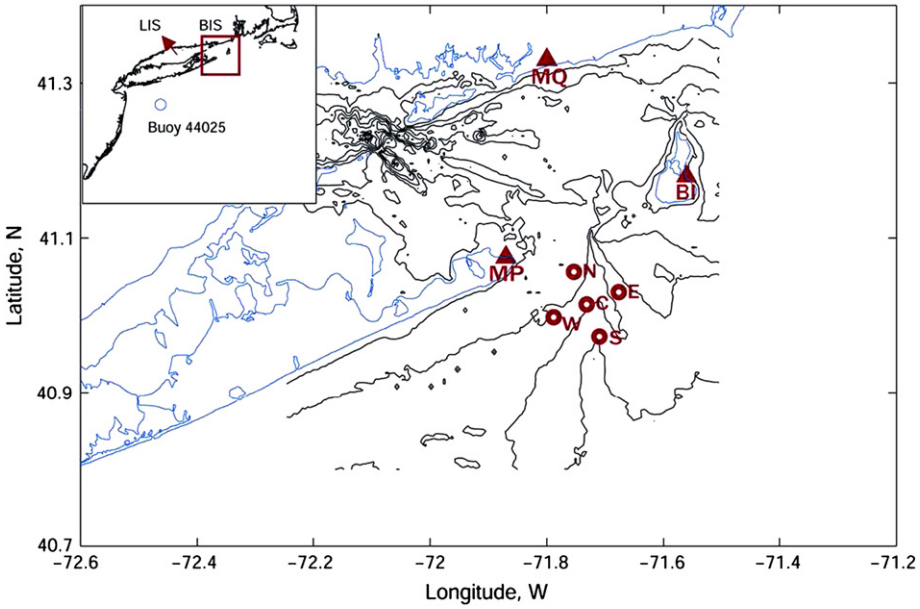

Fig. 1. Triangles are 3 land-based HF radar (CODAR) stations: Montauk Point (MP), Misquamicut (MQ), and Block Island (BI). Circles are 5 ADCP mooring stations. The insert is the map of the New York Bight and Long Island Sound with the weather buoy marked.

York Bight (NYB) (Fig. 1). It is about 45 km long and 40 km wide, and is about 35 m deep near its center. Three openings connect to the BIS. The west opening between LIS and BIS, the Race, is 15 km wide. A deep channel of 80 m deep is in the center of the opening, and the channel is flanked by shallow (10 m) shoals. Deep furrows originate from the channel and extend to the center of BIS. The south opening, the mouth of BIS, is 33 km wide, and a deep submarine canyon sits in the center of the mouth with a maximum depth of 55 m. This submarine canyon extends about 40 km offshore. The east opening with a depth of 25 m connects to the Rhode Island Sound (RIS). A deep channel sits in the opening near the Block Island side, flanked with shallow shoals. The east opening is blocked outside by sills and terraces following the northeast-southwest isobath.

Ullman and Codiga (2004) described the spatial and temporal patterns of surface tidal currents in and outside of BIS based on the HF radar (marketed by CODAR Ocean Sensors) surface velocity measurements of 19 months from June 2000 to December 2001. Codiga and Rear (2004) described the horizontal and vertical structures of the tidal currents at the mouth of BIS based on an array of bottom-mounted ADCPs covering fall 2001 to spring 2002. In BIS, the principal lunar semidiurnal (M_2; 12.42 h period) tidal constituent dominates the current signals and accounts for greater than 80% of the tidal variance. Tidal ellipses generally rotate clockwise in time, and are elongated towards the mouth of BIS. The semi-major axes are largest near the mouth and decrease offshore. In the vertical, tidal currents show characteristic structures of a bottom boundary layer of decreasing amplitude, flattening ellipse, and clockwise turning of major axes towards the bottom.

Numerical models have been used to study the barotropic tides in the NYB. Kenefick (1985) modeled the barotropic M_2 in LIS, forced by the observed tidal elevations at the mouth. He evaluated the model sea levels. Oey et al. (1995) applied a three-dimensional general circulation model to the NYB. They specified the tidal transports at the open boundaries, adjusted to produce the observed costal sea levels. Their model surface tidal currents were compared with historical current meter observations of Mayer et al. (1979). Edwards et al. (2004) also used a three-dimensional model focusing on the LIS outflow. They evaluated the model depth-averaged tidal currents with the moored ADCP observations.

3. Data

Moody et al. (1984) compiled a tidal current and bottom pressure atlas of the U.S. northeast continental shelf from analysis of a large number of historical current meter observations. The atlas includes 19 current meter stations and 15 bottom pressure gauge stations in NYB. The current meter mooring sites are divided into three groups according to the data source (Fig. 4), sites 1–4 (east) are from Flagg et al. (1982), sites 5–11 (middle) from Mayer et al. (1982), and sites 12–19 (west) from Mayer et al. (1979) and Swanson (1976). The surface tidal current data used in this study are from the current meters measured at less than 3 m below the sea surface, and all records are longer than 70 days.

The 15 bottom pressure stations from the Moody atlas are spread over the NYB. We add 8 extra coastal tide stations from New Jersey to Massachusetts, including 3 stations in the LIS. The tidal constants are obtained from the harmonic analysis, and the phase is converted to Greenwich Phase G. The locations of all 23 sea level stations and their tidal constants are listed in Table 1.

Surface currents in BIS have been continuously monitored since June 2000 with three HF radars (CODAR) located at Montauk Point on the eastern tip of Long Island, Misquamicut

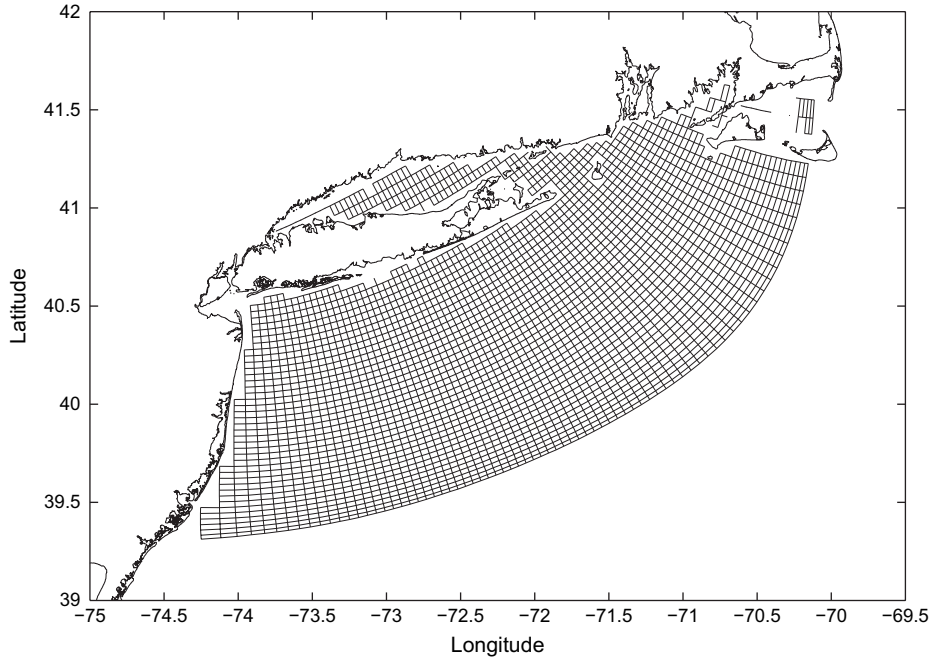

Fig. 2. Model horizontal grid, sub-sampled every third grid point.

at the eastern Rhode Island coast, and Block Island (Fig. 1). The radar has an effective range of about 40 km. Spatial resolution is 1.5 km in the radial direction and 5° in the azimuthal direction. The 25 MHz radar has an effective measurement depth of approximately 0.5 m, and produce hourly maps of radial currents. In regions of overlapping coverage from two or more sites, the least-squares technique of Lipa and Barrick (1986) is used to compute the vector currents within an averaging radius of 2.5 km. Temporal data coverage is quantified by computing the percent of total possible vector returns at each CODAR grid point. Percent coverage decreases rapidly near the edge of the radar coverage. For this reason, a threshold on percent coverage is used to screen out CODAR grid points of less reliable data (Ullman and Codiga, 2004). The CODAR observations used in this study cover a one-year period, from January 1 to December 31, 2001. The time series of east and north surface currents at grid points with percent coverage >10% are used. Missing data are interpolated by optimal interpolation.

Table 1
Tidal elevations for observation and model

Sites	Lon	Lat	Observed amplitude (m)	Phase (degree)	Model amplitude (m)	Phase (degree)
1	−70.67	41.63	0.54	8	0.53	−2
2	−70.77	41.33	0.45	2	0.40	−6
3	−71.05	41.15	0.44	1	0.44	−9
4	−71.32	40.72	0.44	−11	0.44	−9
5	−71.33	41.50	0.51	1	0.50	−9
6	−71.87	40.25	0.47	−12	0.45	−11
7	−71.82	41.08	0.34	11	0.41	−1
8	−72.00	40.20	0.47	−11	0.45	−12
9	−72.25	40.65	0.50	−14	0.47	−13
10	−72.32	40.57	0.48	−13	0.47	−13
11	−72.60	39.95	0.48	−13	0.48	−12
12	−72.63	39.65	0.48	−11	0.46	−11
13	−72.70	39.77	0.50	−9	0.47	−11
14	−72.92	40.12	0.53	−12	0.51	−12
15	−73.23	40.00	0.55	−9	0.53	−11
16	−73.57	40.13	0.59	−10	0.56	−10
17	−73.70	39.63	0.54	−13	0.53	−9
18	−73.50	40.47	0.65	−7	0.57	−12
19	−74.27	39.47	0.59	−2	0.53	−7
20	−74.42	39.35	0.58	−6	0.52	−7
21	−72.09	41.36	0.37	58	0.53	50
22	−73.18	41.17	0.99	110	1.17	87
23	−73.77	40.81	1.14	116	1.31	90

Records from 5 bottom-mounted ADCPs at the mouth of BIS (Fig. 1) during the weakly stratified fall/winter season of fall 2001 also are used in the analysis. The ADCPs are located at water depths between 33 to 55 m. The duration of ADCP records varies, from 70 to 186 days. Vertical resolution is nominally 0.5 m (600 kHz unit) or 1 m (300 kHz unit), and ensemble averaging is nominally over 20 min. Data from the shallowest 2–3 m of the water column are omitted due to acoustic backscatter contamination, and the 2–3 m above the bottom is not sampled. Information on deployments and data reduction is given by Codiga and Houk (2002).

4. Hydrodynamic model

The numerical model used in this study is the Princeton Ocean Model (POM) (Blumberg and Mellor, 1987). The model solves the three-dimensional primitive equations on an Arakawa C grid. The numerical scheme conserves linear and quadratic quantities like mass and energy. The model uses sigma coordinate system in the vertical and orthogonal curvilinear coordinate system in the horizontal. The model

domain extends from Nantucket Sound, MA to Atlantic City, NJ, with one open boundary which arcs between these two locations (Fig. 2). The model topography is sub-sampled from the 3 arc-second gridded East Coast bathymetry archived by the National Geophysical Data Center (NGDC). The model has a total of 151 × 241 × 16 grid points. Horizontal resolution varies from less than 1 km near the coast to about 2 km at the open boundary. In the vertical, the water column is divided into 16 equally spaced levels. The minimum water depth is set at 1 m.

The barotropic model simulation assumes constant temperature and salinity. The vertical eddy viscosity is computed using Mellor and Yamada (1982) level-2.5 turbulence closure scheme, and horizontal eddy viscosity is calculated using shear-dependent Smagorinsky formulation (Smagorinsky, 1963) with a coefficient of 0.2. Bottom friction coefficient and background viscosity are set to 0.0025 and 10^{-5} m^2/s, respectively. At the open boundary the model is driven by the M_2 tidal elevation whose amplitude and phase are linearly interpolated from the Moody atlas. The model also can be forced by the elevation and transport together using the Flather radiation condition; the transport at the open boundary is obtained from a separate model run forced by the elevation only. For the internal mode, the Orlanski radiation condition is used.

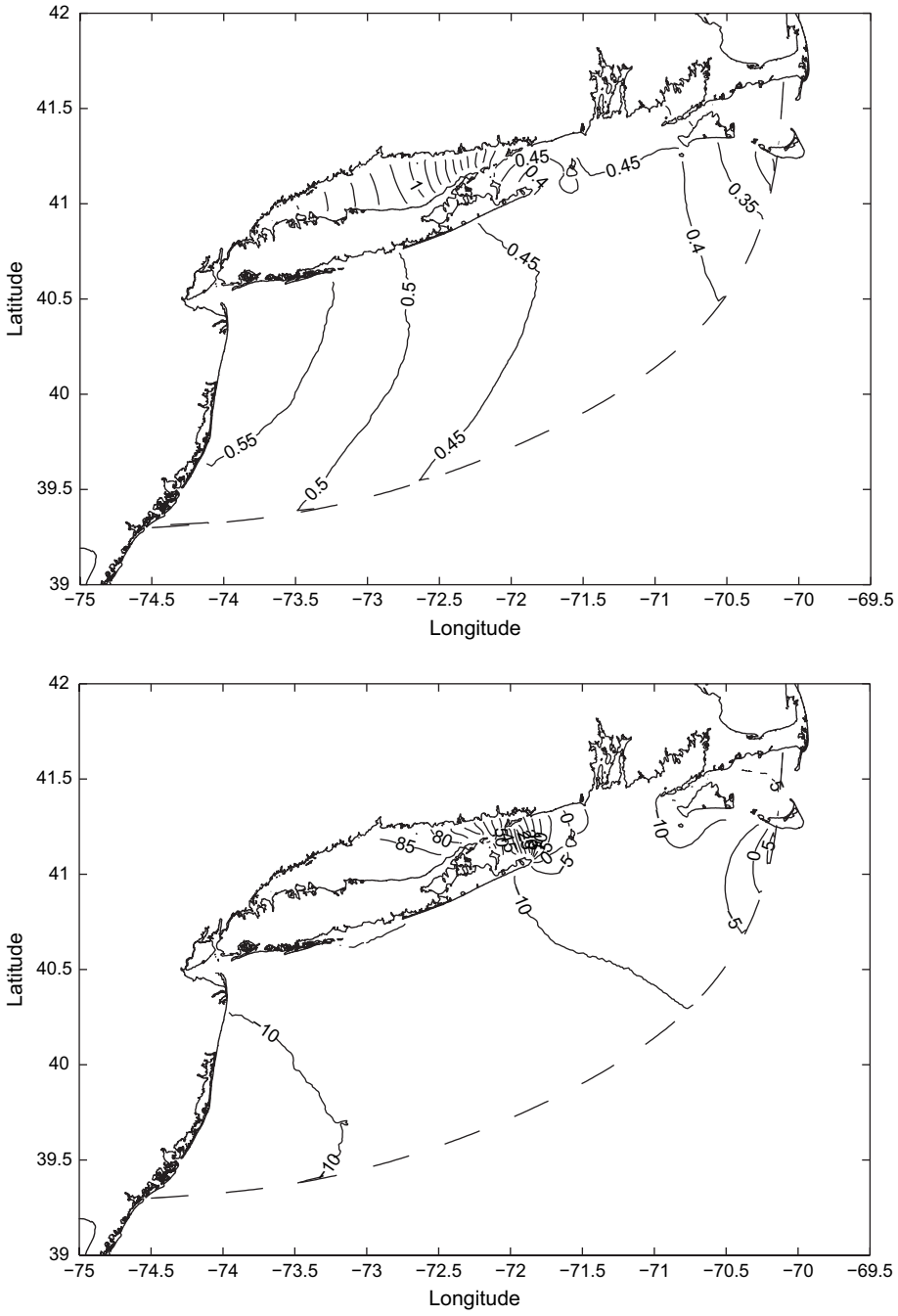

Fig. 3. Model M_2 semidiurnal tides: co-amplitude (m) and co-phase (degree; relative to the Greenwich meridian) lines.

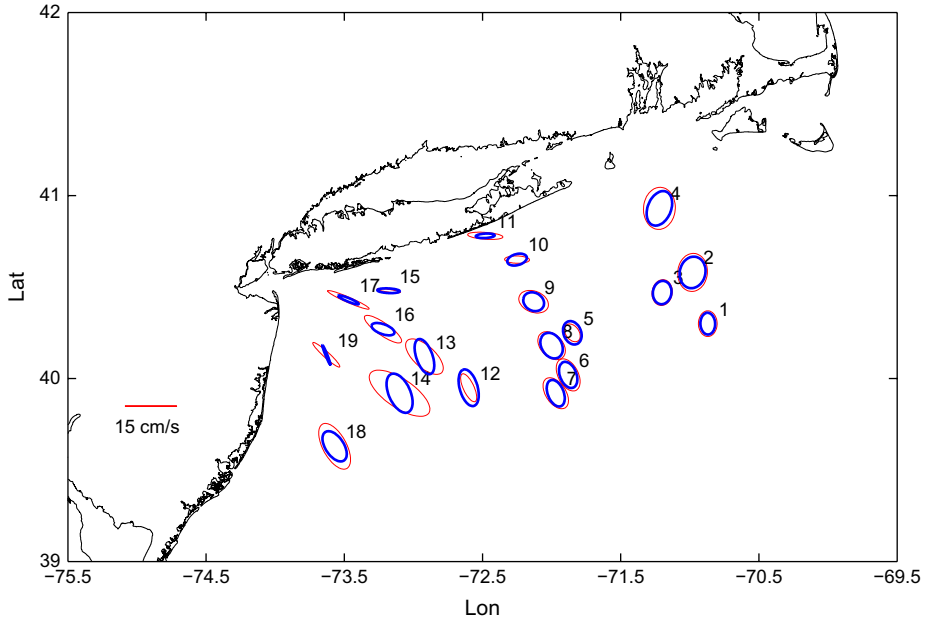

Fig. 4. Comparison of M_2 tidal ellipses in New York Bight between model (blue, thick line) and current meter observations (red, thin line). The depth contours are marked.

Model run begins from a state of rest (zero velocity and elevation), and is run for 15 days to reach a quasi-periodic state.

The tidal amplitude, phase, and current ellipse parameters are calculated based on the least-squares harmonic analysis following Moody et al. (1984). The M_2 tidal ellipses are presented in terms of the four ellipse parameters: semi-major axis (always a positive quantity), semi-minor axis (can be positive or negative; for positive/negative values, the velocity vector traces the tidal ellipse in a counterclockwise/clockwise direction), orientation angle of semi-major axis (counterclockwise from the east), and phase.

5. Model − data comparison

Fig. 3 shows co-amplitude and co-phase lines of M_2 tidal elevations. The model results in the NYB agree well with Swanson (1976) and Moody et al. (1984). The phase ($\sim$350°) and amplitude ($\sim$40 cm) are very nearly constant in NYB. There is however a noted amplitude minimum (30–40 cm) near Nantucket Island. The observed and model elevation amplitudes and phases are listed in Table 1. The errors are small in the NYB, typically <3 cm in amplitude and 4° in phase. However, there is significant error in the LIS (sites

Table 2
Tidal current ellipse parameters for moored current meter observations and model currents

Site	Lon	Lat	Observed semi-major (cm/s)	Semi-minor (cm/s)	Orient (degree)	Phase (degree)	Model semi-major (cm/s)	Semi-minor (cm/s)	Orient (degree)	Phase (degree)
1	−70.87	40.30	5.6	−5.4	90	71	4.8	−4.3	96	60
2	−70.98	40.58	8.7	−8.2	28	61	7.7	−6.7	24	50
3	−71.20	40.47	6.0	−5.5	30	88	5.5	−5.0	26	68
4	−71.22	40.93	9.4	−9.0	85	33	8.5	−6.3	87	20
5	−71.85	40.25	5.0	−3.3	147	−40	5.8	−4.6	142	−46
6	−71.88	40.02	8.3	−5.3	134	−17	6.5	−4.5	129	−45
7	−71.97	39.92	8.6	−5.1	140	−15	6.5	−4.3	127	−44
8	−72.00	40.18	8.5	−5.3	153	−23	6.9	−5.1	150	−39
9	−72.13	40.42	8.7	−4.7	168	−30	6.0	−4.0	168	−16
10	−72.25	40.65	7.2	−1.6	179	−47	5.7	−2.5	190	−20
11	−72.48	40.78	10.2	−1.5	177	−28	5.5	−1.0	182	−6
12	−72.60	39.95	7.1	−2.9	124	−35	8.5	−5.0	115	−39
13	−72.92	40.12	12.3	−5.2	149	9	8.4	−4.5	119	−37
14	−73.10	39.92	19.1	−6.7	155	−7	9.8	−5.8	127	−42
15	−73.18	40.48	6.7	−0.6	174	1	6.5	−1.0	178	−37
16	−73.22	40.27	12.0	−2.9	153	0	6.8	−2.2	156	−40
17	−73.47	40.43	12.6	−1.2	162	−3	6.2	−0.8	153	−46
18	−73.57	39.63	12.1	−6.2	131	−17	8.4	−4.8	138	−46
19	−73.63	40.13	9.4	−1.4	146	−23	4.8	−0.5	148	−40

21–23), which though is outside of the region of interest. The larger error is due to the less well-resolved bathymetry, especially the cross-channel depth variations, in the LIS (Fig. 2).

Fig. 4 shows model and observed tidal ellipses in the NYB. Tidal ellipses are all traced out clockwise in time and are generally oriented approximately perpendicular to local isobaths. Table 2 lists the ellipse parameters. The tidal currents have considerable spatial variations in amplitude and phase. The model and observed tidal current ellipses are in good agreement for east (1–4) and middle (5–11) sites. Averaged over these 11 locations, the misfits, the absolute differences between model and observation, are 1.7 cm/s in semi-major axis, 1 cm/s in semi-minor axis, 5.2° in orientation, and 18° in phase. However, the discrepancy is relatively large in the New York Apex. Averaged over these 8 locations (12–19), the misfits are 4.3 cm/s in semi-major axis, 0.9 cm/s in semi-minor axis, 12° in orientation, and 32° in phase. Oey et al. (1995) previously had noted a similar discrepancy between their model results and observations in the Apex. It is likely that the data (Aanderaa current meters) in these locations were contaminated by surface waves (Mayer et al., 1979).

The vertical structures of the model tidal ellipses are compared with moored ADCPs (Fig. 5). The seasonal changes to near-surface current ellipses during spring (stratified) conditions (Codiga and Rear, 2004) are not considered because the data are from the fall period only. The major axes of tidal ellipses generally rotate clockwise towards the bottom, and the amplitudes decrease sharply at the bottom. The model and ADCP are generally in excellent agreement. The only obvious discrepancy is for the ellipse orientation at East located in the submarine canyon. Observations show the ellipses aligned in the northwest direction at the surface (about 10° counterclockwise from the north) and turned clockwise to the true north near the bottom. The model ellipses, on the other hand, are aligned always in the northwest direction (about 20°

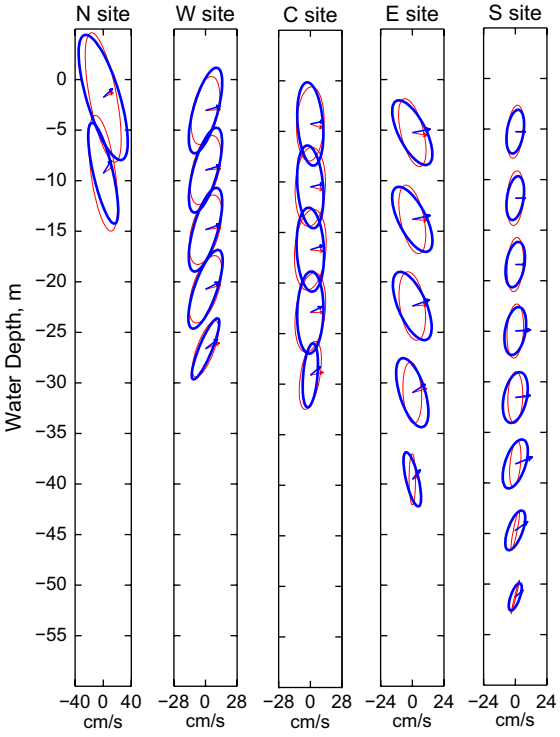

Fig. 5. Vertical structures of M_2 tidal ellipses at 5 ADCP sites: Model (blue, thick line) and ADCP (red, thin line). The phase is marked.

Table 3
Tidal current ellipse parameters for ADCP observations (during fall and winter) and model

	Depth (m)	Model semi-major (cm/s)	Semi-minor (cm/s)	Orient (degree)	Phase (degree)	ADCP semi-major (cm/s)	Semi-minor (cm/s)	Orient (degree)	Phase (degree)
North	−1.78	58.0	14.8	−73	25	58.6	12.1	−80	13
	−9.21	46.3	8.7	−77	38	52.0	10.8	−82	19
West	−3.07	35.0	9.7	75	17	27.4	10.1	79	4
	−8.96	34.7	9.6	74	17	28.0	10.6	77	5
	−14.86	34.3	9.7	74	20	28.3	11.0	75	7
	−20.75	32.8	8.9	71	27	27.8	10.3	72	14
	−26.64	26.0	5.1	68	38	23.8	6.8	70	23
Central	−4.28	33.0	10.0	−85	12	29.4	10.8	−87	−19
	−10.49	32.8	10.1	−85	13	31.4	11.9	−87	−13
	−16.71	33.2	10.7	−87	17	32.1	12.3	−84	−7
	−22.92	32.5	10.3	88	27	31.6	11.6	83	0
	−29.14	25.4	5.6	85	41	27.2	7.7	80	13
East	−5.26	28.1	10.8	−63	11	27.6	9.0	−78	11
	−13.83	28.2	10.9	−63	12	27.6	9.2	−78	4
	−22.40	29.0	11.2	−67	20	27.3	9.8	−82	4
	−30.97	28.4	10.1	−73	33	24.2	7.3	−86	16
	−39.55	21.9	5.0	−77	50	20.2	2.5	−90	28
South	−5.27	17.5	6.6	81	0	21.1	6.3	85	−4
	−11.84	17.7	6.6	81	0	21.7	6.6	86	−2
	−18.41	18.1	7.2	81	1	21.5	6.3	86	−1
	−25.00	19.2	8.1	80	4	21.4	6.4	86	0
	−31.56	20.4	9.1	78	8	20.4	5.9	88	6
	−38.12	20.2	8.1	72	22	18.2	4.2	84	17
	−44.70	16.6	5.8	70	35	16.0	1.5	79	25
	−51.27	11.4	3.4	70	41	13.6	0.5	76	31

counterclockwise from the north). The orientation error likely is due to the unresolved fine-scale topographic features in the canyon. Table 3 lists tidal ellipse parameters at selected depths. The misfits averaged over all 5 ADCPs are 2.8 cm/s in semi-major axis, 1.8 cm/s in semi-minor axis, 6.7° in orientation, and 13° in phase.

6. Model − CODAR comparison

Fig. 6 compares surface currents between CODAR, model, and ADCP at the 5 ADCP sites. The CODAR currents are averages across the shallowest 0.5 m that is weighted toward the surface values, and the ADCP currents are from the shallowest useful bin (1−5 m below the surface). The model and ADCP agree very well as noted above. Except at West where the model semi-major axis is about 7.6 cm/s larger, the amplitude misfits are 2 cm/s for semi-major axis and 1.4 cm/s for semi-minor axis. The agreement between model and CODAR also are good. Averaged over 5 sites, the amplitude misfits between model and CODAR are 7 cm/s for semi-major axis and 5 cm/s for semi-minor axis. It is noted that the agreement between model and ADCP is better than between CODAR and ADCP. This suggests that the model is more accurate than CODAR.

Fig. 6. Comparison of surface M_2 tidal ellipses between ADCP (top), CODAR (middle), and model (bottom) at 5 ADCP sites. The phase is marked.

Fig. 7 compares CODAR and model over the entire CODAR grids. The amplitude misfits are 10.8 cm/s for semi-major axis and 4 cm/s for semi-minor axis, and the orientation misfit is 29°. The misfits show large spatial variations. At the mouth of LIS, for example, the model currents are considerably larger than CODAR. Previous LIS model studies (Kenefick, 1985; Chant, 1991) found maximum tidal currents of about 100 cm/s at the mouth of LIS. Also, Codiga and Aurin (2006) estimated maximum tidal ellipses of 100 cm/s from ferry-based ADCP measurements. The model results of 96 cm/s for semi-major axis and 11 cm/s for semi-minor axis are consistent with those results. This indicates that the large discrepancy is due to poor CODAR data quality at the mouth of LIS.

7. CODAR data quality

The CODAR currents are constructed from the measured radials using vector sum. At a particular location, the vector velocity is obtained from least squares fitting of all available radials located within a 2.5-km radius. To identify the source of CODAR error, it is useful to examine each individual radar radial measurements. Fig. 8 compares radial components of model and CODAR tidal ellipses; model radial ellipses are

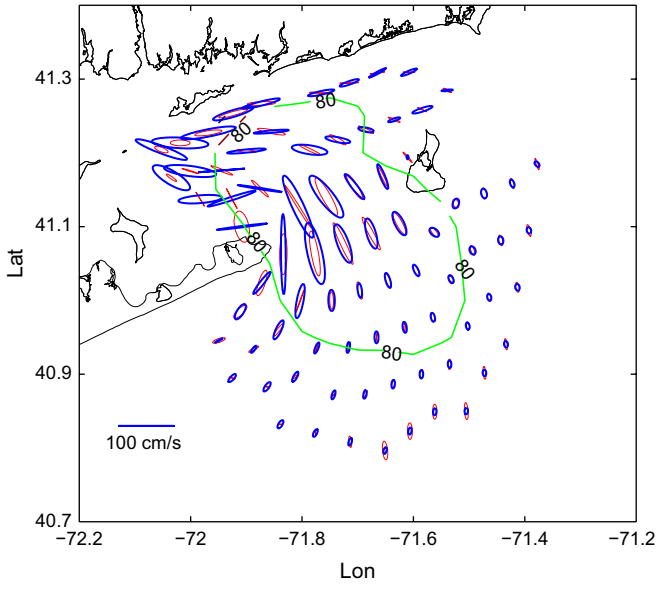

Fig. 7. M_2 tidal ellipses for model (blue, thick line) and CODAR (red, thin line) in Block Island Sound. The data are plotted about every 4th grid point. The 80 percent radar coverage area is marked.

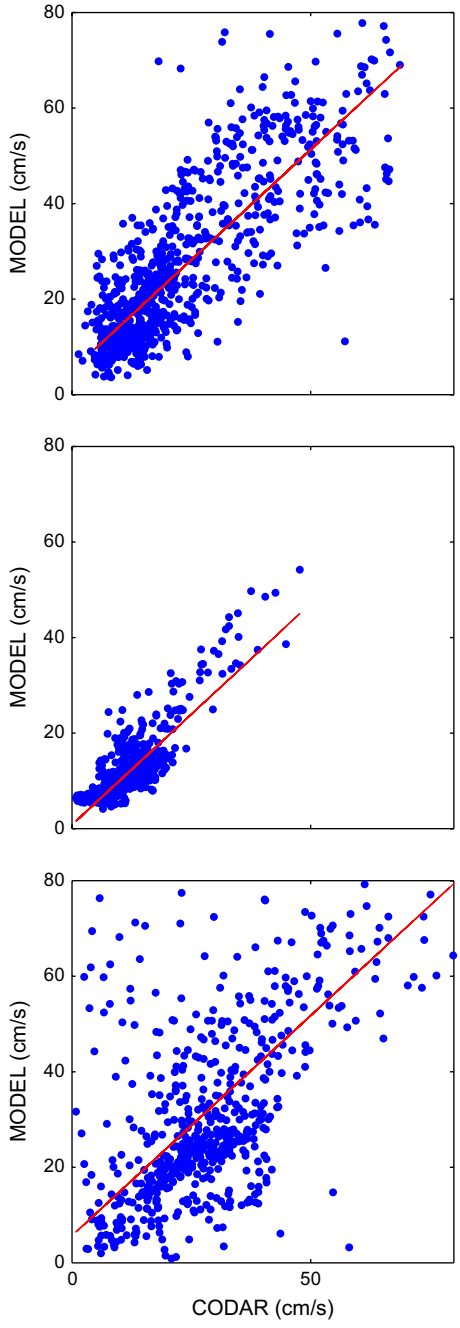

Fig. 8. Comparison between model and CODAR radial components of tidal ellipse at: Montauk Point (top), Block Island (middle), and Misquamicut (bottom). The solid line is the linear regression.

calculated by projecting model currents in the direction of the HF radar. To quantify CODAR error, the bias and rms difference between model and CODAR are calculated. Model and CODAR radials are generally in good agreement at Montauk Point (rms = 9.7 cm/s, bias = 3.4 cm/s, and correlation coefficient $\gamma^2 = 0.82$) and Block Island (rms = 3.5 cm/s, bias = − 0.1 cm/s, and $\gamma^2 = 0.84$), but have large differences (rms = 17 cm/s, bias = 3.3 cm/s, and $\gamma^2 = 0.62$) at Misquamicut. This indicates that Misquamicut is significantly degraded. It is noted that the regression coefficient at all three stations is close to unity (0.92).

The 10% coverage used in the data screening obviously is too generous. We re-calculate the misfits between model and observation using the 80% coverage instead (Fig. 7). The absolute error does not improve because the tidal currents are larger in the 80% coverage area. On the other hand, the relative error, the ratio of the model-data misfit to the model, improves dramatically. The averaged relative error for the ellipse amplitude, $(L_{\mathrm{maj}}^2 + L_{\mathrm{min}}^2)^{1/2}$, is 0.44 in the 10% coverage, but is 0.26 in the 80% coverage. Alternatively, radar data can be screened based on a threshold in the relative error. For example, with cut-off of 0.4, the averaged relative error is about 0.2, and the area mostly overlaps with the 80% coverage.

8. Discussion

Oey et al. (1995) and Edwards et al. (2004) have studied the barotropic tidal currents in the NYB using three-dimensional models. In Oey et al. (1995), the focus is on the New York Apex, and in Edwards et al. (2004) it is on the mouth of BIS. Both studies though only made cursory comparisons of the tidal ellipses. In this study, the model domain encompasses the entire NYB, and the tidal ellipses are systematically evaluated with the current meters, ADCPs, and HF radar. We show that the model results are probably as good as the observations. Our study is possibly the most comprehensive skill assessment of the barotropic tidal currents ever on the U.S. coast.

The scope of our study is compatible to Davies et al. (2001), who made systematic evaluation of the three-dimensional barotropic tidal currents in the Irish Sea. They also utilized ADCP and HF radar (OSCA) for skill assessment; though, their data are not as extensive as used in this study. The tidal regime in the open NYB is quite different from that of the narrow Irish Sea. Our success with NYB suggests that the prediction of coastal tidal currents is well within the reach of the three-dimensional model. On the other hand, model skill assessment at present is still largely restricted to the water levels. We can make great stride towards better understanding of the limitations of the three-dimensional model if more studies will include tidal currents in the skill assessment.

The impact of tidal currents is mainly through tidal mixing, which is most sensitive to the velocity amplitude ($\sim |u|^3$). Thus, in model skill, the phase error is much less critical compared to the amplitude error. Previously, Codiga and Aurin (2006) have applied a one-dimensional oscillatory-boundary layer model to fit the ADCP velocity profile (of fall 2001). Their 'optimal' solution however fails to explain the observed phase increase towards the surface. The three-dimensional model, in contrast, reproduces well the vertical phase lag without fine tuning (Fig. 5). The standard deviations are between 1–5° in 4 out of the 5 ADCP sites; only East has significant error (Table 3). This shows that the bathymetry, which is not considered in the one-dimensional model, is an important factor in determining the phase lag. On the other hand, in calculating the standard deviation, a bias is removed at each site. The phase bias, which has no effect on the vertical structure, presumably is caused by model's failure to simulate the complex horizontal phase pattern over the canyon.

HF radar measurements are subject to many potential errors (e.g., Graber et al., 1997). In comparing 18 pairs of CODAR and vector-measuring current meters (VMCM) off central California, Emery et al. (2004) found wide variations with γ^2 (0.39–0.77) and rms error (7–19 cm/s). While nearsurface vertical shears are real (Dever et al., 1998), there is no explanation for the large scatters in radar error. This indicates that at present it is not feasible to 'calibrate' the radar measurements. Yet, it is generally assumed that the radar-derived tidal (and tidally averaged) currents are trustworthy. This presumption however is far too optimistic. We show that the model tidal currents are more reliable than the radar. We suggest that the tidal model should be used whenever possible to assure the integrity of HF radar measurements.

Acknowledgements

This work was part of the Ph.D. thesis by Jenq-Chi Mau. We appreciate the critical comments from the reviewers.

References

Blumberg, A., Mellor, G.L., 1987. A description of a three dimensional coastal ocean circulation model. In: Neaps, N.S. (Ed.), Three-Dimensional Coastal Ocean Models. American Geophysics Union, pp. 1–16.

Chant, R.J., 1991. The Barotropic tide in Long Island Sound and its response to rise in sea level. Master thesis, State University of New York, Stony Brook, NY, 150 pp.

Codiga, D.L., Aurin, D.A., 2006. Residual circulation in eastern Long Island Sound: observed transverse-vertical structure and exchange transport. Continental Shelf Research, in press. doi:10.1016/j.csr.2006.09.001.

Codiga, D.L., Houk, A.E., 2002. Current Profile Time Series From The FRONT Moored Array, Technique Report, Dep. of Mar. Sci., UCONN, Groton, p. 19.

Codiga, D.L., Rear, L.V., 2004. Observed tidal currents outside Block Island Sound: offshore decay and effects of estuarine outflow. Journal of Geophysical Research 109, C07S05. doi:10.1029/2003JC001804.

Davies, A.M., Hall, P., Howarth, M.J., Knight, P.J., Player, R.J., 2001. Comparison of observed (HF radar and ADCP measurements) and computed tides in the north channel of the Irish Sea. Journal of Physical Oceanography 31, 1764–1785.

Dever, E.P., Hendershott, M.C., Winant, C.D., 1998. Statistical aspects of surface drifter observations of circulation in the Santa Barbara Channel. Journal of Geophysical Research 103 (C11), 24,781–24,797.

Edwards, C.A., Fake, T.M., Bogden, P.S., 2004. Spring-summer frontogenesis at the mouth of Block Island Sound: Part 1, a numerical investigation into tidal and buoyancy-forced motion. Journal of Geophysical Research 109 (C12), C1202. doi:10.1029/2003JC002132.

Emery, B.M., Washburn, L., Harlan, J.A., 2004. Evaluating radial current measurements from CODAR High-Frequency radars with moored current meters. Journal of Atmospheric and Oceanic Technology 12, 1259–1271.

Flagg, C.N., Magnell, B.A., Fry, D., Cura, J., McDowell, S., Scarlet, R., 1982. Interpretation of physical oceanography of Georges Bank, Final Report. EG&G Environmental Consultant Report 82-B459.

Graber, H.C., Haus, B.K., Chapman, R.D., Shay, L.K., 1997. HF radar comparisons with moored estimates of current speed and direction: expected differences and implications. Journal of Geophysical Research 102 (C8), 18,749–18,766.

Kenefick, A.M., 1985. Barotropic M_2 tides and tidal currents in Long Island Sound: a numerical model. Journal of Coastal Research 1, 117–128.

Lipa, B.J., Barrick, D.E., 1986. Least-squares methods for the extraction of surface currents from CODAR crossed-loop data: application at ARSLOE, IEEE. Journal of Oceanic Engineering OE-8, 226–253.

Lynch, D.R., Davis, A.M., 1995. Quantitative Skill Assessment for Coastal Ocean Models. American Geophysics Union, 510 pp.

Mayer, D.A., Hansen, D.V., Ortman, D.A., 1979. Long-term current and temperature observations on the Middle Atlantic Shelf. Journal of Geophysical Research 84, 1776–1792.

Mayer, D.A., Han, G.C., Hansen, V.D., 1982. Circulation in the Hudson Shelf Valley: MESA physical oceanographic studies in New York Bight. Journal of Geophysical Research 87 (C12), 9563–9578.

Mellor, G.L., Yamada, T., 1982. Development of a turbulence closure model for geophysical fluid problems. Reviews of Geophysics and Space Physics 20, 851–875.

Moody, J.A., Butman, B., Beardsley, R.C., Brown, W.S., Daifuku, P., Irish, J.D., Mayer, D.A., Mofield, H.O., Petrie, B., Ramp, S., Smith, P., Wright, W.R., 1984. Atlas of Tidal Elevation and Current Observations on the Northeast American Continental Shelf and Slope. U.S. Geological Survey Bulletin 1611, 122.

Oey, L.-Y., Manning, H.T., You, K.W., 1995. A plume and wind driven circulation model of the New York Bight. In: Lynch, D.R., Davies, A.M. (Eds.), Quantitative Skill Assessment for Coastal Ocean Models. American Geophysics Union, pp. 329–347.

Smagorinsky, J., 1963. General circulation experiments with the primitive equations. Part I: the basic experiment. Monthly Weather Review 91, 99–164.

Swanson, R.L., 1976. Tides. MESA, 4; New York Sea Grant Institute, 44 pp.

Ullman, D.S., Codiga, D.L., 2004. Seasonal variation of a coastal jet in the Long Island Sound outflow region based on HF radar and Doppler current observations. Journal of Geophysical Research 109, C07S06. doi:10.1029/2002JC001660.

Whitney, M.M., Garvine, R.W., 2006. Simulating the Delaware Bay buoyant outflow: comparison with observations. Journal of Physical Oceanography 36, 3–21.